Effects of Shape and Mass Properties on Subsonic Dynamics of Planetary Probes

George L. Cahen*
Martin Marietta Corporation, Denver, Colo.

Introduction

As an atmospheric instrument platform, it is desirable for a planetary probe to exhibit a steady, zero angle of attack and minimal buffeting due to unsteady flow separation and impingement in the afterbody region. Of the many high drag probe shapes reported in the literature,[1-8] each exhibits a limit cycle and/or a buffeting behavior during some portion of the Mach number range. The most satisfactory shape yet discovered is that used for the Planetary Atmospheric Entry Test[9] (PAET) program by the NASA Ames Research Center. The PAET vehicle was a blunted, 110° cone forebody with an approximately hemispherical afterbody centered on the vehicle center of gravity (c.g.). During the flight, the PAET vehicle experienced lateral buffeting from a Mach number of 4 on down.

To define a more satisfactory passive probe configuration, static and dynamic tests in conventional wind tunnels (MMC Denver and Colorado State University), a water column (Ames), a vertical wind tunnel (Langley) and a ballistic range (Ames) including a large number of shapes have been conducted. The dynamic tests included studies of the effects of c.g. location and pitch radius of gyration (σ). This Note concerns only the work done in the vertical wind tunnel (Langley Spin Tunnel).

Models

The shapes tested are shown in Fig. 1. The models were constructed of fiberglass reinforced plastic about 1/32 in. thick with a central screw upon which various combinations of weights were located so as to provide variations in c.g. and pitch radius of gyration. This scheme is illustrated in Fig. 2. The pitch radius of gyration for each configuration tested was confirmed through use of a torsional pendulum arrangement. Because of volume limitations inside the models and total weight limitation (by the operating speed of the tunnel, $V_{cont} = 60$ fps), it was not possible to produce identical values of radius of gyration for the various configurations. All models had a maximum diameter of 10 in. and one, a 90-deg forebody with the F afterbody, was also tested with a maximum diameter of 24 in.

Tests

The tests consisted of "floating" the models in the spin tunnel and perturbing them with an external force in order to study the dynamic behavior. The only data obtained consisted of motion pictures which included a clock and a wind speed meter. As the models moved about in the tunnel, they were manually tracked with the movie camera, which was gimbal mounted.

The motion pictures have been analyzed by measuring the model attitude as a function of time as indicated by the clock image on each frame. Readings were not made during periods when the wind velocity was changing rapidly. Thus the limit cycle angle, the angle to which the model could be disturbed without tumbling and, for some models, the angle which would produce tumbling, could be determined.

The results obtained for all the configurations for the three significant angles mentioned previously are summarized in Tables 1-3 for the 90-, 110-, and 120-deg forebodies, respectively. If sufficiently disturbed, all of the models except the one indicated in Table 1 (D) would tumble. The entry "Tumble" in the tables indicates that the model automatically entered a divergent oscillation and eventually tumbled. The entry "Lift" in the tables indicates that the model moved laterally in the tunnel, hitting the wall and would not remain steady enough to permit disturbing it.

Perusal of the tables will indicate that the effect of moving the c.g. forward and of increasing the value of d/σ is particularly evident in changing the behavior from tumbling to limit cycle. In some cases there appears to be a reversal in the effect of d/σ; however, this is probably due to inaccuracy of the data, about ± 2 deg. In Tables 1 and 3, for the 90- and 120-deg forebodies, the F afterbody exhibits the smallest limit cycle angles, but in Table 2, for the 110-deg forebody, the E afterbody shows the minimum values. This anomalous result may also be an inaccuracy effect.

It is especially interesting that in Table 1, the large F model showed a 0 deg limit cycle angle. The different behavior for the 10-in. and 24-in. models may be due to the scale of turbulence in the wind stream. It is not believed to be a Reynolds number effect because the drag coefficients deduced for the two models were identical. There was a slight difference in the geometry of the two models in that the center of curvature of the aft spherical segment for the 10-in. model was at the base plane of the forecone and that for the 24-in. model was located 5% d ahead of this plane.

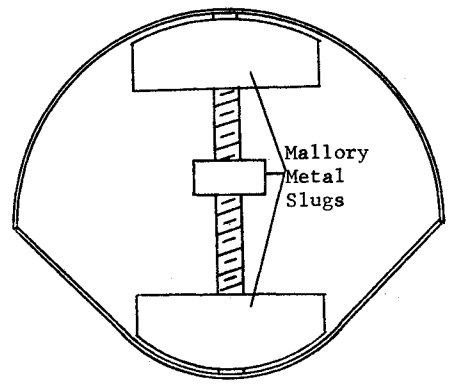

Fig. 1 Configurations tested, showing code letters used in the tables.

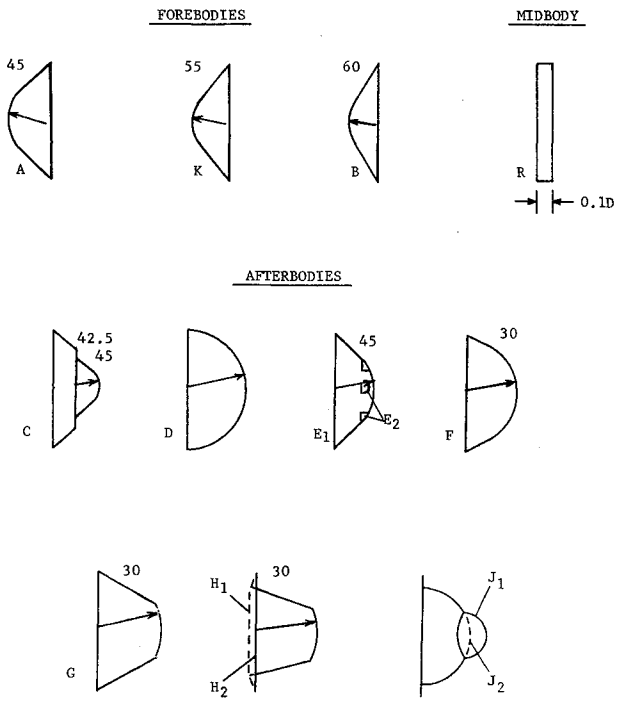

Fig. 2 Schematic showing internal arrangement of models.

Received March 24, 1975; revision received May 27, 1975.
Index categories: Entry Vehicle Dynamics and Control; Entry Vehicles and Landers.

*Senior Group Engineer. Associate Fellow AIAA.

Table 1 Summary of spin tunnel results for 90° cones

Config/c.g.	0.0% d				−2.5% d		−4.0% d	−5.0% d		
C	Tumble[a] 3.6									
D	15-will not tumble 3.5				Lift 4.1			Lift 3.9		
E_1					10-40-X 4.6	6-30-X 5.0		6-24-45 3.6	2-45-X 4.4	
E_2	Tumble 3.5		Tumble 5.2	9-40-X 3.8	5-44-X 4.6	6-40-X 5.0		10-42-50 3.6	4-25-X 4.4	
E_2-R		35-X-X 4.3		28-X-X 3.5	12-12-X 4.2			10-X-X 3.4	6-20-X 4.0	
F	2-35-X 3.8		4-35-X 4.9	5-40-X 3.6	3-40-X 4.0	5-40-X 4.7	4-45-50 4.0	4-45-X 3.5	5-80-X 3.8	5-45-X 4.6
F (24 in.)							0-30-50 4.0			
F-R	6-15-X 3.5	7-32-X 4.2		10-30-X 3.4	7-12-X 4.0			5-36-X 3.3	5-23-X 3.9	
G					7-40-X 4.0				12-70-X 3.9	
G-R				15-X-X 3.6				15-32-X 3.5		
J1		Tumble 4.6	Tumble 5.4	12-X-30 3.6	6-35-X 4.5	3-25-X 5.3		4-29-40 3.8		5-45-X 5.0
J2	Tumble 3.8		Tumble 5.1	5-38-X 3.6		6-40-X 5.3		5-40-X 3.9		

[a]Note: Behavior Code → a-b-c a) Limit cycle half angle, degrees; b) Maximum angle obtained without tumbling; c) Angle for tumbling. d/σ.

Table 2 Summary of spin tunnel results for 110° cones[a]

Config/c.g.	−3.5%		−10.0% d
E_1	36-X-X 3.6	2-36-48 4.8	0-56-X 3.9
F	4-46-78 3.6	5-49-65 4.6	3-67-X 3.9
H_2		24-X-37 4.9	

[a]See footnote, Table 1.

It is possible for a vehicle to experience lateral accelerations due to buffeting on the afterbody without exhibiting angle of attack oscillations. As there were no acceleration measurements for this test program, this question cannot be ansered. More detailed studies of this configuration including flow visualization and accelerometer measurements would seem to be in order.

References

[1] Jaffe, P., "Dynamic Stability Tests of Spinning Entry Bodies in the Terminal Regime," *Journal of Spacecraft and Rockets,* Vol. 8, June 1971, pp. 575-579.

Table 3 Summary of spin tunnel results for 120° cones[a]

Config/c.g.	0.0%			−2.5% d			−3.5% d
D		10-X-X 4.6		15-X-X 3.5	12-X-X (Lift) 4.6		
E_1	Tumble 3.9	8-35-X 4.8	4-41-52 5.6		7-X-65 4.6	5-59-62 5.5	
E_2	Tumble 3.9	15-21-38 4.8	6-X-50 5.6	Tumble 3.7	5-39-50 4.6	5-X-60 5.5	
F	Tumble 3.5	10-34-25 4.3	2-40-X 5.5	6-44-50 3.6	2-55-X 4.6	9-44-X 5.4	
F-R	20-40-X 3.5	3-38-X 4.6		4-29-X 3.6	5-X-X 4.5		
G				15-20-30 3.6	5-20-X 4.6		
G-R					7-X-X 4.0		
H_1							5-60-68 4.9
H_2							5-52-58 4.9
J1					7-23-X 4.6	5-48-X 5.4	
J2					5-16-X 4.9		

[a]See footnote, Table 1.

[2]Marko, W. J., "Transonic Dynamic and Static Stability Characteristics of Three Blunt-Cone Planetary Entry Shapes," JPL TR32-1357, Sept. 1969, Jet Propulsion Lab., Pasadena, Calif.

[3]Sammonds, R. I., "Dynamics of High-Drag Probe Shapes at Transonic Speeds," TN D-6489, Sept. 1971, NASA.

[4]Krumins, M. V., "Drag and Stability of Mars Probe/Lander Shapes," *Journal of Spacecraft and Rockets,* Vol. 4, Aug. 1967, pp. 1052-1057.

[5]Cassanto, J. M. and Brice, P., "Free Fall Stability and Base Pressure Drop Tests for Planetary Entry Configurations," *Journal of Spacecraft and Rockets,* Vol. 8, July 1971, pp. 790-793.

[6]Costigan, P. J., "Dynamic-Model Study of Planetary-Entry Configurations in the Langley Spin Tunnel," TND-3499, July 1966, NASA.

[7]Marte, J. E. and Weaver, R. W., "Low-Subsonic Dynamic Stability Investigation of Several Planetary-Entry Configurations in a Vertical Wind Tunnel—Parts I and II," JPL TR-32-743, May 1965, Jet Propulsion Laboratory, Pasadena, Calif.

[8]Short, B. J., "Dynamic Flight Behavior of a Ballasted Sphere at Mach Numbers from 0.4 to 14.5," TN-D-4198, Oct. 1967, NASA.

[9]Seiff, A., Reese, D. E., Sommer, S. C., Kirk, D. B., Whiting, E. E., and Niemann, H. B., "PAET, an Entry Probe Experiment in the Earth's Atmosphere," *Icarus,* Vol. 18, April 1973, pp. 525-563.

Elevation Stepping of Gimballed Devices on Rotor-Stabilized Spacecraft

Gerald J. Cloutier*
M.I.T. Lincoln Laboratory, Lexington, Mass.

Introduction

THE pointing accuracy of dual-spin or momentum-wheel stabilized spacecraft can be affected by gimballed sensors which perform scanning motions. These motions can induce nutation of the vehicle. Particularly in cases involving rapid elevation steps in the motion of gimballed sensors, computer simulation of the resulting spacecraft motion can be complex, requiring extensive reprograming for each case considered. A graphical technique is described in this Note which permits rapid evaluation of the effects of a stepping sensor on the motion of the basic spacecraft.

Basic Gimballed Appendage Motions

The dynamic system used to illustrate spacecraft response to gimballed scan sensor perturbations consists of a rotor-stabilized spacecraft with gimballed appendage (Fig. 1). The vehicle is assumed to have equal transverse moments-of-inertia; i.e., it is symmetric about the spin-axis of the rotor. Gimballed appendage motion can be categorized in two types: azimuth motions, which are rotations about an axis parallel to the vehicle's spin axis, and elevation motions, which are rotations about a transverse axis. Azimuth motions interact directly with the spin control system of the rotor. Studies of these interactions require detailed simulation of the spin control system. Of more immediate interest here are elevation motions that do not interact with the interbody control loop, except in cases involving product-of-inertia coupling of platform azimuth and nutation motions. Otherwise, the main effect of elevation motions of an articulated appendage is to cause the spacecraft to nutate.

Received March 28, 1975; revision received May 21, 1975. This work was sponsored by the U.S. Air Force.

Index category: Spacecraft Attitude Dynamics and Control.

*Staff Member. Member AIAA.

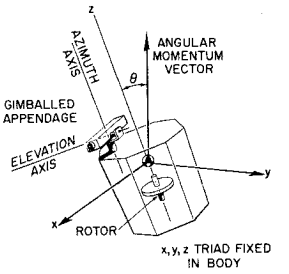

Fig. 1 Spacecraft with gimballed appendage.

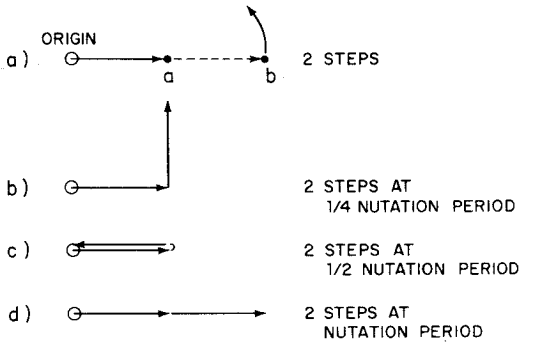

Fig. 2 Nutation step sequences.

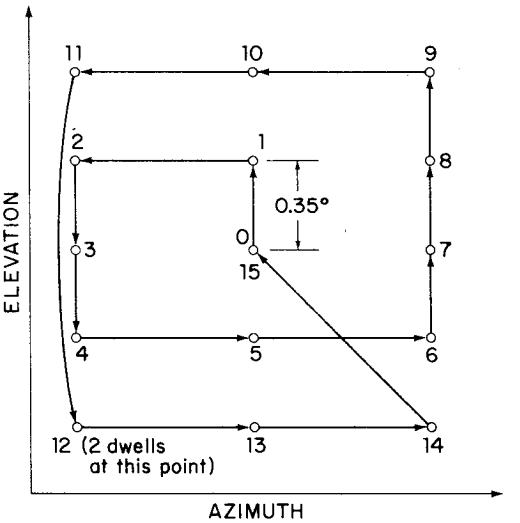

Fig. 3 Search scan pattern.

If an appendage, such as the device shown in Fig. 1 is stepped an angle, ϕ, in a very short time (i.e., short compared with the natural nutation period of the spacecraft), it impulsively induces a nutation of the spacecraft. The amount of nutation, measured by nutation angle Θ between the spacecraft's spin axis and the angular momentum (Fig. 1) is proportional to the angle ϕ, the constant of proportionality being the ratio of transverse inertias, i.e.,

$$\Theta = (I/J_T)\phi \tag{1}$$

where J_T is the transverse inertia of the spacecraft, and I is the transverse inertia of the device. If, after some time, a second elevation step occurs, it induces an additional nutation. However, this change in nutation angle will occur at some phasing relative to the original, since the spacecraft's z-axis will have been coning about the angular momentum vector because of the initial nutation. Thus, analysis of the effects of a series of steps can become complicated.

Nutation Coordinate System

A convenient method for following spacecraft motions during a sequence of appendage elevation steps has been devised. Essentially a graphic technique, it involves defining a